

Global Consistent Point Cloud Registration Based on Lie-algebraic Cohomology

Yuxue Ren¹, Baowei Jiang², Wei Chen³, Na Lei^{3,*}, Xianfeng David Gu⁴,

1 Academy for Multidisciplinary Studies, Capital Normal University

2 Beijing Advanced Innovation Center for Imaging Theory and Technology, Capital Normal University

3 DUT-RU ISE, Dalian University of Technology

4 State University of New York at Stony Brook

* correseponding nalei@dlut.edu.cn

Abstract

We present a novel, effective method for global point cloud registration problems by geometric topology. Based on many point cloud pairwise registration methods (e.g ICP), we focus on the problem of accumulated error for the composition of transformations along any loops. The major technical contribution of this paper is a linear method for the elimination of errors, using only solving a Poisson equation. We demonstrate the consistency of our method from Hodge-Helmhotz decomposition theorem and experiments on multiple RGBD datasets of real-world scenes. The experimental results also demonstrate that our global registration method runs quickly and provides accurate reconstructions.

keywords Global Point Cloud Registration, Lie-algebraic cohomology, Hodge-Helmhotz decomposition, graph theory

1 Introduction

Motivation Recent years have witnessed the rapid development of Structure from Motion (SfM) [5, 8, 10, 32] and Simultaneous Localization And Mapping (SLAM) [19, 20, 26, 38]. Many global reconstruction methods have been proposed, among them the most traditional ones are the sequential approaches, which iteratively add new data to 3D models from point cloud collections. In practice, sequential approaches are expensive, because they require repeated nonlinear model refinement (bundle adjustment) [2, 24]; they are error-prone, since they may lead to error accumulation and exacerbate the drifting effects.

To improve the consistency, the fundamental concept of *viewing graph* has been developed. The viewing graph encapsulates the point clouds treated as nodes and the relative transformations between the point clouds as edges. *Global consistency* is defined as concatenating transformations along each loop in the graph. It should return the identity under the assumption of an ideal noise-free setting.

Based on the viewing graph, many iterative reconstruction methods have been proposed [8, 10, 23, 31, 34]. These methods consider all relative poses of point clouds (e.g. edges of the graph), simultaneously estimate all poses in a single step and restrict the focus on cycles in the graph structure [8, 26, 38, 44]. Although sophisticated techniques have been applied, such as nonlinear optimization [9, 26] and [14, 17, 37, 44] rotation averaging, the existing methods cannot achieve global consistency with high precision, only obtain rough approximated solutions. Our goal is to propose a novel algorithm to tackle the loop close problem and greatly improve the global consistency.

Our Solution In this work, we approach the global consistency problem from a fundamentally different perspective: *the viewing graph is treated not as a solely 1-skeleton graph, but a higher dimensional Cech complex, namely it has much richer topological information, encoded by the Cech cohomology, which is the key to solve the loop closing problem.*

Contribution This work proposes a novel algorithm to tackle the loop closing problem based on Lie-Algebraic Cech cohomology, the contributions include:

1. Our method is different with other graph optimization method, based on Helmholtz-Hodge decomposition theorem, the loop closing problem can be solved through solving a system of linear equations.
2. The viewing graph is generalized to a Cech complex to enrich the topological structure.
3. The relative rigid motion on the edges is formulated as a Lie-algebraic simplicial 1-form, thus the loop closing condition is equivalent to the exactness of the 1-form.
4. The exact component of the Lie-algebraic 1-form can be extracted using Helmholtz-Hodge decomposition algorithm.
5. The 2-skeleton of the Cech complex can be approximated by graph embedding.

Furthermore, our experimental results demonstrate the simplicity, efficiency and accuracy of the proposed algorithm.

The remainder of the paper is organized as follows: the related works are reviewed in Sec. 2; the elementary concepts are introduced in Sec. 3; the computational algorithms are explained in Sec. 4, including Cech complex construction, graph embedding, Lie-algebra valued 1-form and Hodge decomposition; the experimental results are reported in Sec. 5; and eventually the paper is concluded in Sec. 6.

2 Related Work

In this section, we review the most related approaches for solving the loop closing problem. There are mainly three types of algorithms: matrix methods, averaging rotation and translation, graph optimization.

Matrix Methods Arie-Nachimson [28] constructed a $3n \times 3n$ symmetric matrix by concatenating the pairwise rotation matrices and then used either the spectral decomposition or the semidefinite programming (SDP) method to compute the set of global rotations. Arrigoni [15] also views the absolute rotation estimation problem as a low-rank and sparse matrix decomposition for the above symmetric matrix by Bilateral Random Projections (BRP). They calculated the rotation and the translation separately. In contrast, our method computes the rotation and the translation simultaneously.

Averaging Rotation Govindu [44–46] and Chatterjee [1] used the lie-algebraic averaging method to control the drift due to the accumulating error and the estimated camera motion. Hartley [36,37] gave a provably convergent algorithm for finding the L^1 mean of $SO(3)$ under several relative orientation measurements. The work in [17] proposed edge weights method to average rotation. All the above works decouple translations from rotations. Purkait [33] viewed relative orientations, i.e. rotation between two frames, as the edge features, then proposed the view-graph cleaning network (CleanNet) and fine-tuning network (FineNet), which built on Message-Passing Neural Networks (MPNN), to predict outlier edges and refined absolute orientations respectively. Taking the average can ensure consistency along special loops, but it is not clear whether the consistency holds for all the loops. The proposed Hodge decomposition method can guarantee global consistency along any loop of the viewing graph.

Graph Optimization Snavely [23] used a graph algorithm-based maximum leaf spanning tree (MLST) to select a skeletal subset of images and finally used bundle adjustment, which aimed at reducing the computation redundancy. And Lim [23] proposed a system consisting of a local as well as a global adjustment on the online environment mapping, which obtains a key-frame pose graph from a key-frames subset. Sprickerhof [26] proposed a vertex weights algorithm to optimize the graph by removing edge. For the learning method, the set of edges with the bad relationship can be inferred

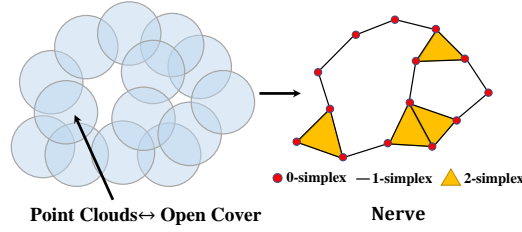


Figure 1. Construction of Cech complex

by a Bayesian framework in [8]. This type of methods destroy the original viewing graph, therefore lose partial topological information of the Cech complex. Compared to the existing methods, our proposed method achieves high accuracy, and the optimized viewing graph does not require any filtering steps to remove “bad” relative poses [8, 23, 31]. Hence, our algorithmic pipeline is simpler and more efficient than alternative approaches [26, 37, 44].

Helmholtz-Hodge Decomposition Theorem The well-known Helmholtz-Hodge decomposition theorem [18, 27, 29] claims that any differential 1-form on a Riemannian manifold can be decomposed into three orthogonal components, an exact form (curl free), a co-exact form (divergence free) and a harmonic form (both curl free and divergence free). Namely, each cohomological class has a unique harmonic form. Therefore, we can extract the exact component from the initial Lie-algebraic 1-form. Unlike existing methods [7, 12, 40, 44, 45], our algorithm mentioned in Section 4 solves global rotations and translations simultaneously linearly.

3 Theoretic Background

3.1 Cech Complex and Cech Cohomology

In the viewing graph, each point cloud is treated as a node, two overlapping point clouds are represented as an edge, three point clouds mutually intersecting each other should be represented as a 2-dimensional face (2-simplex) in the Cech complex, similarly each k -order cliques in the viewing graph is a k dimensional simplex in the Cech complex. The Cech complex enriches the topological and the algebraic relation of the viewing graph [35]. In more detail, let $\mathfrak{U} = \{U_\alpha\}_{\alpha \in J}$ be a set of point clouds, where the index set J is a countable ordered set. Every U_α can also be regarded as an open set embedded in 3D space from the geometric point of view. Denote the intersection set $U_\alpha \cap U_\beta$ as $U_{\alpha\beta}$, etc. The definition of Cech complex is as follows:

Definition 1 (Cech complex) The Cech complex of \mathfrak{U} is a simplicial complex constructed as follows. To every open set U_α , we associate a vertex α . If $U_{\alpha_0} \cap U_{\alpha_1}$ is nonempty, we connect the vertices α_0 and α_1 with an edge, if $U_{\alpha_0} \cap U_{\alpha_1} \cap \dots \cap U_{\alpha_n}$ is non empty, we say $\alpha_0, \alpha_1, \dots, \alpha_n$ construct an n dimensional cell of the Cech complex etc. For the basics of simplicial complexes, see [16].

A function defined on k -dimensional simplicial of Cech complex is represented as a k -form, all of this kind of functions form a topological space, i.e., Cech Cohomology.

Cech Cohomology Let $\Omega^0(U)$ be the vector space of const functions on U , and $\Omega^1(U)$ be the space of 1-forms on U , etc. Let $C^0(\mathfrak{U}, \mathbb{R}) = \prod_{\alpha_0} \Omega^0(U_{\alpha_0})$ be the connection of all const functions on U_α , and $C^1(\mathfrak{U}, \mathbb{R}) = \prod_{\alpha_0 \alpha_1} \Omega^0(U_{\alpha_0 \alpha_1})$ be the connection of const functions on all $U_{\alpha_0 \alpha_1}$. Following a similar approach, $C^{n+1}(\mathfrak{U}, \mathbb{R}) = \prod_{\alpha_0 \dots \alpha_{n+1}} \Omega^0(U_{\alpha_0 \dots \alpha_{n+1}})$ can be defined the connection of const functions on all $U_{\alpha_0 \alpha_1 \dots \alpha_{n+1}}$. For $\omega \in C^p(\mathfrak{U}, \mathbb{R})$, and $\partial_q : C^p(\mathfrak{U}, \mathbb{R}) \rightarrow C^{p+1}(\mathfrak{U}, \mathbb{R})$, define the boundary operator as

$$(\partial_q \omega)_{\alpha_0 \dots \alpha_{p+1}} = \sum_{i=0}^{p+1} (-1)^i \omega_{\alpha_0 \dots \hat{\alpha}_i \dots \alpha_{p+1}}. \quad (1)$$

Definition 2 (Cocycle) A cochain $\omega \in C^q(\mathfrak{U}, \mathbb{R})$ is the ∂_q -cocycle that satisfies $\partial_q \omega = 0$, namely the kernel of ∂_q .

Definition 3 (Coboundary) A cochain $\omega \in C^q(\mathfrak{U}, \mathbb{R})$ is called ∂_q -coboundary, if there exists a $\omega' \in C^{q-1}(\mathfrak{U}, \mathbb{R})$ satisfies $\partial_{q-1}\omega' = \omega$, namely the image of ∂_{q-1} .

In this problem, the Lie-algebraic of the relative rigid motion on the edges of Cech complex is formulated as a simplicial 1-form, and loop closing condition corresponds to an exact 1-form, i.e., a 1-form satisfying cocycle condition.

3.2 Cocycle Condition

Let $\{\omega_{\alpha\beta} : U_{\alpha\beta} \rightarrow \mathbb{R}, \forall U_{\alpha\beta}\}$ be a 1-form defined on edges of Cech complex, for the transition function $\{\omega_{\alpha\beta}\}$ of the open cover \mathfrak{U} , if they satisfy

$$\omega_{\alpha\beta} \circ \omega_{\beta\gamma} = \omega_{\alpha\gamma} \quad \text{on} \quad U_{\alpha} \cap U_{\beta} \cap U_{\gamma}, \quad (2)$$

for any open subsets $U_{\alpha}, U_{\beta}, U_{\gamma} \in \mathfrak{U}$, then $\{\omega_{\alpha\beta}\}$ satisfies the co-cycle condition. In more general cases, for U_{α_i} , where $\alpha_i \in J, i = 1, \dots, n$, co-cycle condition is

$$\omega_{\alpha_0\alpha_1}\omega_{\alpha_1\alpha_2}\cdots\omega_{\alpha_{n-1}\alpha_n} = \omega_{\alpha_0\alpha_n}. \quad (3)$$

When the set of point clouds are registered together, the error accumulation of local registration between point clouds leads to large errors for the first and last point clouds in a closed loop. This error is essentially the product of transformations on the closed loop, not the identity mapping. The condition requires that the product of transformation on any closed loop is identical mapping, so that any closed loop has global consistency.

From the view of the Cech cohomology above, coboundaries, satisfy the cocycle condition naturally, but the cocycles may not. In other words, if a transition function $\{\omega_{ij}\}$ of \mathfrak{U} is a coboundary, then the product on every closed loop is identity.

The next section introduces the way to compute a coboundary from a cocycle.

3.3 Lie Algebras of the relative rigid motion

All the rigid motions form a Lie group, the tangent space at the identity form the Lie algebra. Since the rotation matrix is not commutative, during the process of our algorithm, the Lie algebras of the Rotation and Euclidean groups should be used. For rotation $R \in SO(3)$, its lie-algebra $\phi \in \mathbb{R}$ satisfy $R = \exp(\phi^\wedge)$, where

$$\phi^\wedge = \begin{bmatrix} 0 & -\phi_3 & \phi_2 \\ \phi_3 & 0 & -\phi_1 \\ -\phi_2 & \phi_1 & 0 \end{bmatrix}. \quad (4)$$

Then for rotation $R \in SO(3)$ and translation $t \in \mathbb{R}^3$, their lie-algebra $[\phi, t] \in \mathbb{R}^6$, is Abelian. Thus the 6D vector on the graph is our motion field. For each oriented edge of the complex, we associate a rigid motion with it, which can be estimated by the iterative closest point (ICP) algorithm. Then we further represent the rigid motion as a vector in the Lie algebra. Therefore we can treat the rigid motions defined on all the edges as a Lie-algebraic simplicial 1-form on the Cech complex, then use the Lie-algebraic simplicial cohomology to rephrase the loop close problem: the integration of the Lie-algebraic 1-form is zero along any closed loop (1-chain), this implies the 1-form is exact, namely it is the gradient of some function defined on the Cech complex.

3.4 Graph Embedding

The topological structure of the Cech complex is complicated, involving high dimensional simplexes. For Hodge decomposition, only 2-skeleton is needed. Therefore, we can embed the view graph on a surface, and use the surface to approximate the 2-skeleton of the Cech complex and perform the Hodge decomposition. This method preserves the algebraic property of the viewing graph [22], ensures the loop closing condition and improves the efficiency.

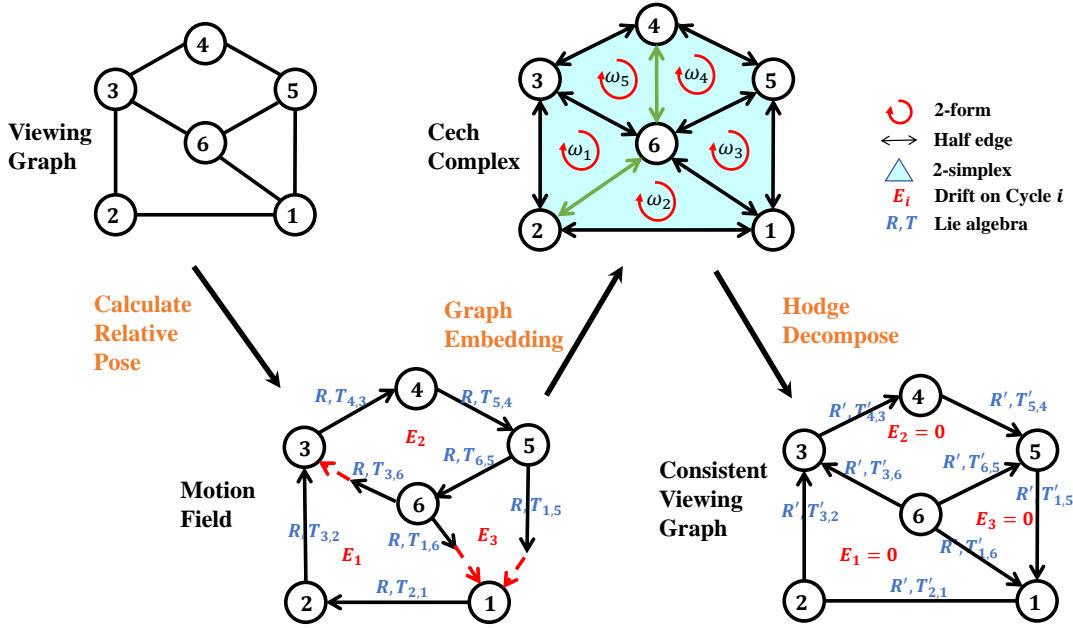


Figure 2. Hodge Algorithms Pipeline. a) Construct viewing graph by SIFT (if the number of matches is more than 50, add the corresponding edge), b) calculate Lie algebra of rigid transform from ICP, c) triangularization by graph embedding, 4) solve curl free field by solving equation 8. Finally, we realize consistency.

An embedding of G is a map $f : G \rightarrow S$, such that each edge $e \in E_G$ is mapped to a simple arc on the surface, and these arcs don't intersect at the interior points [21, 41]. It is well known that embedding a graph onto a surface with a fixed genus is linear time in the graph size and doubly exponential in the genus [4], while finding the embedding surface with the minimal genus is NP-hard [6]. For the current purpose, we choose a linear algorithm and do not pay attention to minimizing the genus.

4 Computational Algorithms

In this section, we explain our algorithmic pipeline in detail, Fig 2 lists the pipeline.

Cech Complex Construction The viewing graph $G = (V_G, E_G)$ is constructed as usual, each node in V_G represents a point cloud, the corresponding camera frame is called a pose. The point clouds are roughly registered using ICP or NDT algorithm. Each edge in E_G represents two intersecting point clouds, and is associated with the transformation between the two poses associated with the end nodes. The viewing graph is the 1-skeleton of the Cech complex. Each k -clique (k -complete sub-graph) of the viewing graph represents a k -dimensional simplex in the Cech complex, its boundary consists of all the $k - 1$ sub-cliques. The Cech complex is denoted as Σ .

Graph Embedding The Cech complex Σ has a complicated topological structure, we can embed the viewing graph onto a surface and use the embedding surface to approximate the 2-skeleton of Σ . For each vertex $v \in V_G$, we randomly define a cyclic order for all the edges adjacent to v , denoted as e_0, e_1, \dots, e_{n-1} . For each edge we define two half-edges h_k^+ and h_k^- , where the target vertex of h_k^+ is v and the source vertex of h_k^- is v . After defining the cyclic orders for all the vertices and constructing all the halfedges, we connect the halfedges as follows: for each vertex v and for each k , we connect h_k^+ to h_{k+1}^- , where $k + 1$ is modulo n . After connecting all the halfedges, if we start an arbitrary halfedge, and trace it by the connection, we will go through a loop and return to the initial

Algorithm 1 Graph Embedding

Input: A 3-connected Graph $G = (V_G, E_G)$
Output: A surface S and an embedding $f : G \rightarrow S$

For each vertex v

 Define a cyclic order of edges adjacent to v ;

 Attach two opposite halfedges h_k^+, h_k^- to each edge e_k ;

 The target vertex of h_k^+ is v ; Connect h_k^+ to h_{k+1}^- ;

End For
For All halfedge h

 Trace h to form a loop;

End For

Each loop gives a cell; All the cells are glued by the edges to form a surface S ;

Triangulate the surface S .

Algorithm 2 Rigid Transformation Form

Input: The viewing graph $G = (V_G, E_G)$;

the embedding surface S ;

the rigid motions defined on G , ω_0 .

Output: The rigid transformation form ω defined on S .

For each edge e in S

 If e is not in G

 Find the shortest path $\gamma \subset G$ connecting the two end vertices of e ;

 Define $\omega(e)$ as the integration of ω_0 along γ ;

 End If
End For

halfedge. Namely, we have divided all the halfedges into disjoint loops, each loop is a 2-dimensional topological cell. All the cells are glued together by the edges to form an oriented closed surface. This linear algorithm gives one embedding surface of the graph G , denoted as S . Furthermore, we can triangulate each cell and convert S and obtain a topological triangulation of S . We represent S as a triangle mesh. The details can be found in Alg.1.

Rigid Transformation 1-Form Each edge of the viewing graph is associated with a relative point cloud transforming the point clouds associated with the two end nodes, which are obtained by point cloud registration. The transformations on the edges don't satisfy the loop closing condition, we have to compose the transformation on each edge with a small adjustment to meet the constraint. The small adjustment for the relative transformation on each edge is a differential rigid motion, denoted as $\omega = (\omega_1, \omega_2)$, where $\omega_1 : E_G \rightarrow \mathfrak{so}(3)$ is the rotation component taking the value in the Lie-algebra $\mathfrak{so}(3)$, $\omega_2 : E_G \rightarrow \mathbb{R}^3$ the translation component. ω is treated as a Lie-algebraic 1-form defined on Σ . Consider each edge e in the triangle mesh S , if e is in the viewing graph G , then $\omega(e)$ has been calculated already. If e is not in the graph G , then on the graph G there is the shortest path γ connecting the two vertices of e , therefore, we define $\omega(e)$ equals to the integration of ω along γ , namely

$$\omega(e) = \int_{\gamma} \omega = \sum_{e_i \in \gamma \subset E_G} \omega(e_i). \quad (5)$$

The details of the algorithm can be found in Alg.2.

Hodge Decomposition

Theorem 4 (Hodge Decomposition Theorem) For any $\omega \in C^q(\mathfrak{U}, \mathbb{R})$, there is a unique

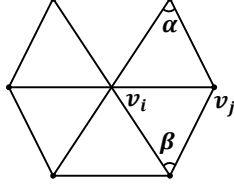


Figure 3. Cotangent weight $w_{ij} = \frac{1}{2}(\cot\alpha + \cot\beta)$.

decomposition as

$$\omega = df + \delta g + h. \quad (6)$$

where df is an exact form, δg is a co-exact form and h is a harmonic form.

According to Helmholtz-Hodge theorem, $\omega = (\omega_1, \omega_2)$ can be decomposed into the sum of an exact form, a co-exact form and a harmonic form, and the decomposition is unique. The work of [27] gives an algorithm to extract the harmonic component from a given 1-form. In this work, we apply the similar method, from Eqn. 6, we have

$$\delta\omega = \delta df + \delta^2 g + \delta h = \Delta f, \quad (7)$$

therefore the function f satisfies the Poisson equation.

In the discrete setting, the above Poisson equation can be formulated as: for each vertex $v_i \in S$,

$$\Delta f(v_i) := \sum_{v_i \sim v_j} w_{ij}(f(v_j) - f(v_i)), \quad (8)$$

where $v_i \sim v_j$ means v_j is adjacent to v_i , and w_{ij} is the well known cotangent weighting coefficients [30, 42, 47] as shown in Fig. 3. Similarly, the co-boundary operator is

$$\delta\omega(v_i) = \sum_{v_i \sim v_j} w_{ij}\omega([v_i, v_j]). \quad (9)$$

In our case, the cotangent weight is calculated under a special constant metric, see Fig. 3, all of the edges have an equal length 1. It can be shown that the exact form extraction is independent of the choice of the metric. The exact component $df = (df_1, df_2)$ of $\omega = (\omega_1, \omega_2)$ can be obtained by directly solving the Poisson equation Eqn. 7 using Eqn. 8 and Eqn. 9.

5 Experimental Evaluations

In this section, the experimental results are reported, which demonstrate the efficiency and accuracy of our global consistency optimization algorithm.

5.1 Datasets

The proposed algorithm has been evaluated on datasets from several different sources, including synthetic data with ground truth, real world data captured by handheld Kinect scanner and the geometric point clouds captured by our stereo-camera system with structured light.

ICL-NUIM Dataset consists of eight synthetic RGBD video sequences: four from an office scene and four from a living room scene, provided by Handa et al. [3]. The real camera pose information, obtained by the Kintinuous system [43], allows us to accurately assess the accuracy of our reconstruction. We conducted experiments on two input sequences, Living room 2 and Office 2, for a thorough comparison.

7-Scenes Dataset released by Shotton et al [25], consists of seven indoor scenes. All seven scenes were shot with a handheld Kinect RGB-D camera and “ground truth” camera tracks were captured by the KinectFusion system [39].

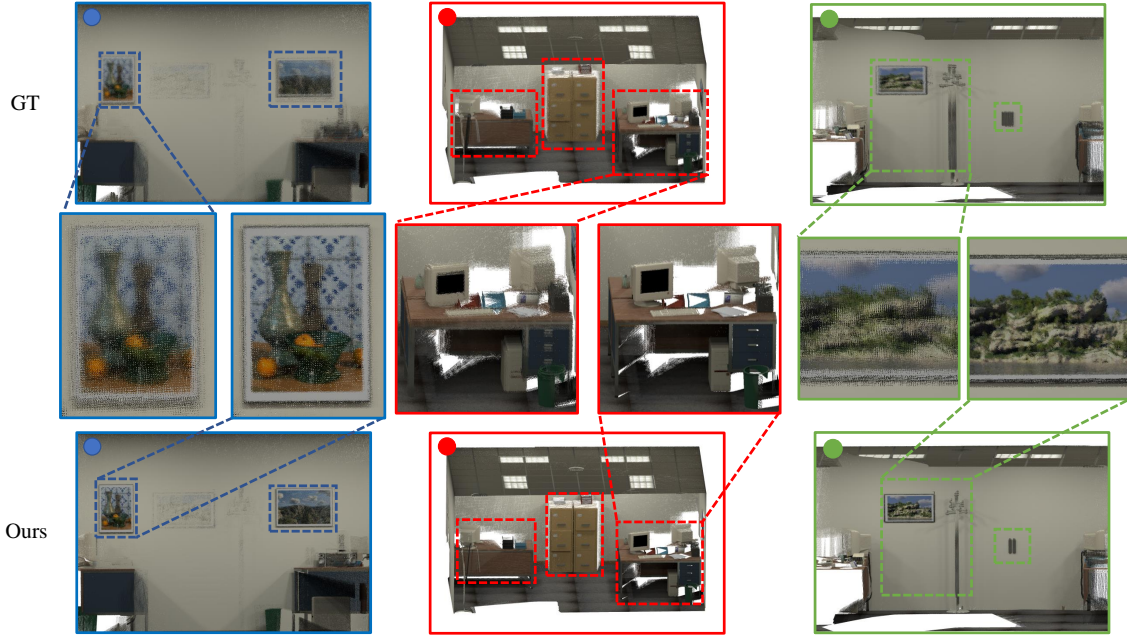


Figure 4. Comparison between our method and the “ground truth” (GT) of the Office 2 scene in the ICL-NUIM dataset. Top row: the reconstruction by the GT trajectory provided by the KinectFusion. Affected by the simulated sensor noises, the GT are imperfect. Bottom row: the registration result by our method. It can be seen that our method produces sharper details in the middle row. This demonstrates that our approach achieves higher quality.

5.2 Evaluation Procedure

Quantified Evaluation In order to quantitatively evaluate our method, we first construct the viewing graph based on two metrics, the centroidal distance and the intersection over union (IOU) [13]. We calculate the two metrics for each pair of point clouds. For a given pair, if the centroidal distance is less than a threshold or the IOU is greater than a threshold, then we add an edge corresponding to the pair of point clouds to the viewing graph.

For each edge in the viewing graph, we compute the *negative exponential power of the point-2-plane distance* [11] between the two point clouds corresponding to the end nodes. The score is normalized to the unit interval, the higher score means the higher registration accuracy.

Experimental Results As explained in the algorithm section 4, our algorithm computes the initial Lie-algebraic 1-form ω using the ICP algorithm, then performs Helmholtz-Hodge decomposition by solving the Poisson Eqn. 7 to extract the exact component df . Then df is applied to update the poses and fuse the point clouds with high global consistency. If we want to further improve the global consistency and the reconstruction accuracy, we can repeat the whole procedure on the updated poses. Multiple iterations can be applied to achieve higher quality.

For the comparison purpose, we transform the input point clouds (frames) along the available “ground truth” trajectory provided by the KinectFusion system or the Kintinuous system, and denote the results as the “ground truth” reconstructions.

We compare the reconstruction results obtained by different algorithms, including the “ground truth” (GT), the BundleFusion (BF) [2], and our Hodge decomposition algorithm with one iteration (Hodge 1st) and three iterations (Hodge 3rd). The comparison results are summarized in Table 1 and Table 2.

In Table 1, the viewing graph is constructed based on the centroidal distance among the point clouds, each edge corresponds to a pair of point clouds with centroidal distance less than 0.2 meter. The scores of the negative exponential power of the point-2-plane distance on all the edges are

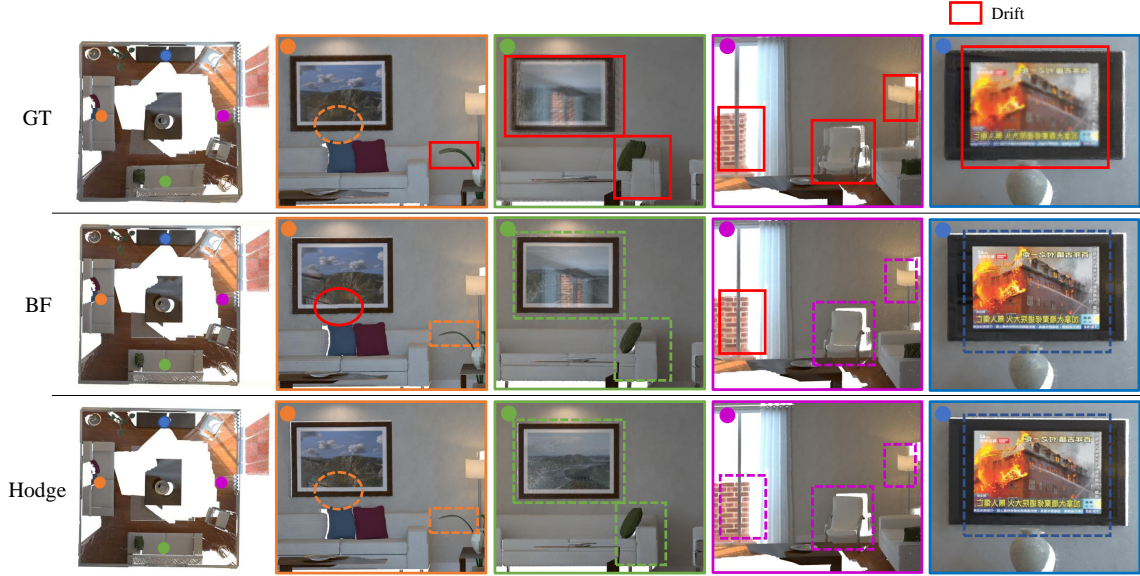


Figure 5. Comparison among the “ground truth”, the BundleFusion [2] and our algorithm on the Living Room 2 scene in the ICL-NUIM dataset. Top row: the reconstruction (point cloud) by the “ground true” and the four local details (saffron:painting and plants, green:painting and sofa, purple:Balcony,armchair and lamp, blue:TV). Middle row: the reconstruction by the BundleFusion algorithm. Bottom row: the reconstruction by our method. The solid red box indicates poor reconstruction due to the drifting effect, and the dotted box indicates the better results. It can be observed that our approach has the least drifts and highest global consistency.

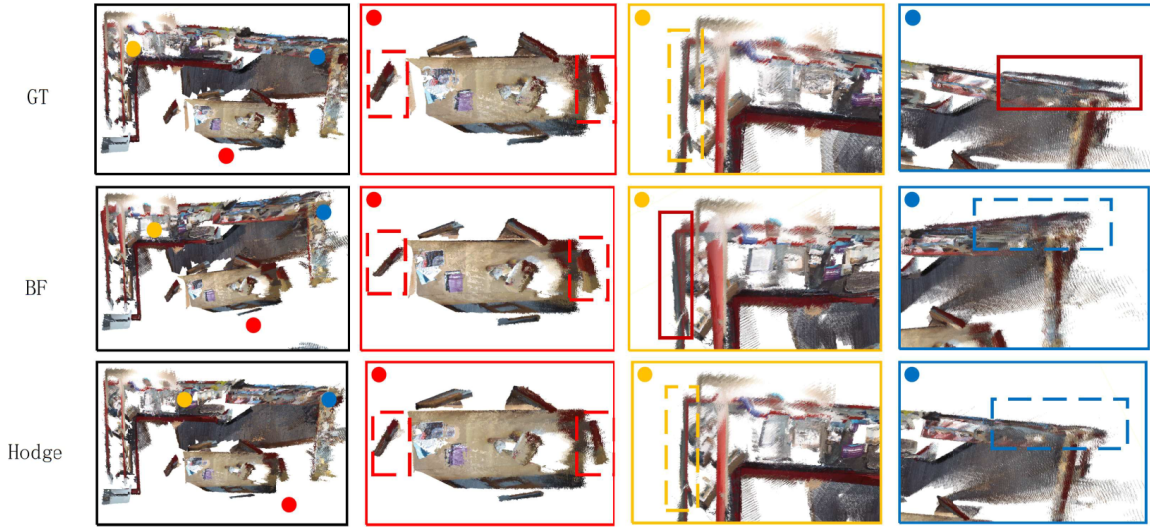


Figure 6. Comparison of the “redkitchen” scene. Top row: the reconstruction (point cloud) by the “ground truth” and three local details (table, corner of upper left and right wall). Middle row: the reconstruction by the Bundle-Fusion algorithm. Bottom row: the reconstruction by our method. The solid red curves mean the failure regions, the broken curves mean the regions without drifting. Numerically and visually, our method outperforms others.

Table 1. On the viewing graph under Euclidean metric, the average negative exponential power of the point-2-plane distance of ground truth, BundleFusion and Hodge method of iteration one and three time. The score’s upper bound is 1, the larger the better.

	GT	BF	Hodge 1st	Hodge 3rd
chess	0.829	0.827	0.827	0.827
fire	0.869	0.868	0.870	0.869
redkitchen	0.863	0.865	0.865	0.865
stairs	0.821	0.818	0.822	0.822
living2	0.803	0.883	0.921	0.918
office2	0.783	nan	0.931	0.937

Table 2. On the viewing graph under IoU metric, the average score of ground truth, BundleFusion and Hodge method of iteration one and three time. The score’s upper bound is 1, the larger the better.

	GT	BF	Hodge 1st	Hodge 3rd
chess	0.837	0.835	0.836	0.838
fire	0.870	0.868	0.870	0.870
redkitchen	0.862	0.864	0.864	0.865
stairs	0.818	0.814	0.820	0.820
living2	0.805	0.878	0.919	0.915
office2	0.781	nan	0.930	0.935

averaged, the average scores for different algorithms are reported in the table. All the computations are with 6 decimal precision, and the final results are rounded to reduce the redundancy. The best scores are in bold font. It can be seen that for 5 of the 6 examples, our proposed Hodge decomposition algorithm outperforms both the ground truth and the BundleFusion algorithm.

Similarly, in Table 2, the viewing graph is constructed based on the intersection over union among the point clouds, each edge corresponds to a pair of point clouds with IOU greater than 0.5. Our proposed method also outperforms the other two methods for 5 of the 6 examples. This demonstrates that our method can achieve higher reconstruction accuracy.

Note that in both cases, BundleFusion algorithm fails for reconstructing the office2 dataset, hence the pose for each frame can not be obtained. Hence its scores in both tables are labeled as nan.

Furthermore, we also explicitly evaluate the global consistency by computing the integration of the Lie-algebraic 1-form along different loops as follows: first, we compute a set of the basis loops $\{\gamma_i\}_{i=1}^{2g}$ of the first homology group of the embedding surface $H_1(S, \mathbb{Z})$, and integrate ω along each base loop. Each integration result $\int_{\gamma_i} \omega$ is a rigid motion. We compute the L^2 norm of the translation component, and the Frobenius norm of the rotation component minus the identity matrix, the total norm measures the deviation of the rigid motion from the identity. We report the results below, which demonstrates the high global consistency (loop closedness) of our method.

Fig. 4 shows the comparison between our proposed algorithm and the “ground truth” on the ICL-NUIM dataset. It can be seen that the reconstruction of our method has higher quality and shows finer local details. Fig. 5 and Fig. 6 shows the comparison among ground truth, BundleFusion [2] and our algorithm on the ICL-NUIM dataset. By examining the reconstruction details, one can see that our method achieves the best quality and has the least drifting effects.

Consistency Verification We choose m loops in the view graph, $\gamma_1, \gamma_2, \dots, \gamma_m$. Suppose γ_k has n_k edges $\{e_{i,i+1}\}_{i=0}^{n_k-1}$, the rigid motion on the edge e_{ij} is denoted as M_{ij}^k . The composition of the rigid motion along γ_k is given by $\Pi_{i=0}^{n_k-1} M_{i,i+1}^k$. We measure the deviation of the composed rigid

Table 3. Loop consistency on ICL-NUIM and 7-Scenes dataset

	living2	office0	office2	office3	redkitchen	chess	other
Hodge 1	3e-4	4.16e-2	3e-4	1.0463e-1	7.28e-2	1.5e-4	0.00
Hodge 2	0.00	2e-5	0.00	0.00	0.00	0.00	0.00
Hodge 3	0.00	0.00	0.00	0.00	0.00	0.00	0.00

motions from the identity for all the loops, and denoted it as

$$D := \sum_{i=1}^m \|\Pi_{i=0}^{n_k-1} M_{i,i+1}^k - I_4\|_F. \quad (10)$$

where I_4 is the fourth order identity matrix. Deviation $D = 0$ means that the relative poses are consistent along all loops, i.e. they satisfies the global consistency condition: loop closedness.

For the ICL-NUIM and 7-Scenes dataset, we list all the deviations D 's in Eqn. 10 of three iterations of our Hodge decompose algorithm, denoted as Hodge 1, Hodge 2 and Hodge 3 respectively in Table 3.

In Table 3, it can be seen that among the first 6 examples, the Hodge decomposition with one iteration obtains relative large deviations, by increasing the iterations, the global consistency is greatly improved, two or three iterations can achieve zero deviations D 's.

6 Conclusions

This work introduces a novel algorithm to tackle the challenging loop closing problem in global point cloud registration. The algorithm generalizes the viewing graph to a Cech complex with richer topological structure, and treat the relative transformations defined on the edges as a Lie-algebraic simplicial 1-form on the Cech complex, then use Helmholtz-Hodge decomposition to extract the exact component of the 1-form, which gives the relative transformations among the frames. Furthermore, the 2-skeleton of the Cech complex can be approximated by an embedding surface of the viewing graph.

Experimental results demonstrate the simplicity, efficiency and accuracy of the algorithm. It outperforms the conventional methods and achieves higher global consistency.

However, this algorithm assumes the relative transformations on each edge in the viewing graph is in the neighborhood of the identity in the Lie group of the rigid motion, hence it can be represented using a vector in the Lie algebra. If the poses are sparse, and the relative transformations are far away for the identity, the Lie-algebraic representations are inaccurate. The proposed method will encounter difficulties. In the future, we will explore further to overcome this shorting coming.

References

1. A.Chatterjee and V.Govindu. Efficient and robust large-scale rotation averaging. In *2013 IEEE International Conference on Computer Vision*, pages 521–528, 2013.
2. A.Dai, M.Nießner, M.Zollhöfer, S.Izadi, and C.Theobalt. Bundlefusion: Real-time globally consistent 3d reconstruction using on-the-fly surface reintegration. *ACM Transactions on Graphics (ToG)*, 36(4):1, 2017.
3. A.Handa, T.Whelan, J.McDonald, and A.Davison. A benchmark for rgb-d visual odometry, 3d reconstruction and slam. In *2014 IEEE International Conference on Robotics and Automation (ICRA)*, pages 1524–1531, 2014.
4. B.Mohar. A linear time algorithm for embedding graphs in an arbitrary surface. *SIAM Journal on Discrete Mathematics*, 12(1):6–26, 1999.

5. C.Sweeney, T.Sattler, T.Höllerer, M.Turk, and M.Pollefeys. Optimizing the viewing graph for structure-from-motion. In *2015 IEEE International Conference on Computer Vision (ICCV)*, pages 801–809, 2015.
6. C.Thomassen. The graph genus problem is np-complete. *Journal of Algorithms*, 10(4):568–576, 1989.
7. C.Tomasi and T.Kanade. Shape and motion from image streams under orthography: a factorization method. *International journal of computer vision*, 9(2):137–154, 1992.
8. C.Zach, M.Klopschitz, and M.Pollefeys. Disambiguating visual relations using loop constraints. In *2010 IEEE Computer Society Conference on Computer Vision and Pattern Recognition*, pages 1426–1433, 2010.
9. D.Borrmann, J.Elseberg, K.Lingemann, A.Nuchter, and J.Hertzberg. Globally consistent 3d mapping with scan matching. *Robotics and Autonomous Systems*, 56:130–142, 02 2008.
10. D.Crandall, A.Owens, N.Snaveley, and D.Huttenlocher. Discrete-continuous optimization for large-scale structure from motion. In *CVPR 2011*, pages 3001–3008, 2011.
11. D.Landry, F.Pomerleau, and P.Giguère. Cello-3d: Estimating the covariance of icp in the real world. In *2019 International Conference on Robotics and Automation (ICRA)*, pages 8190–8196, 2019.
12. D.Martinec and T.Pajdla. Robust rotation and translation estimation in multiview reconstruction. In *2007 IEEE Conference on Computer Vision and Pattern Recognition*, pages 1–8, 2007.
13. D.Zhou, J.Fang, X.Song, C.Guan, J.Yin, Y.Dai, and R.Yang. Iou loss for 2d/3d object detection. In *2019 International Conference on 3D Vision (3DV)*, pages 85–94, 2019.
14. F.Arrigoni and A.Fusiello. Synchronization problems in computer vision with closed-form solutions. *International Journal of Computer Vision*, 128(1):26–52, 2020.
15. F.Arrigoni, L.Magri, B.Rossi, P.Fragneto, and A.Fusiello. Robust absolute rotation estimation via low-rank and sparse matrix decomposition. In *2014 2nd International Conference on 3D Vision*, pages 491–498, 2014.
16. F.Croom. *Basic concepts of algebraic topology*. Springer Science & Business Media, 2012.
17. G.Sharp, S.Lee, and D.Wehe. Multiview registration of 3d scenes by minimizing error between coordinate frames. *IEEE Transactions on Pattern Analysis and Machine Intelligence*, 26(8):1037–1050, 2004.
18. H.Bhatia, G.Norgard, V.Pascucci, and P.Bremer. The helmholtz-hodge decomposition—a survey. *IEEE Transactions on Visualization and Computer Graphics*, 19(8):1386–1404, 2013.
19. H.Lim, J.Lim, and H.Kim. Real-time 6-dof monocular visual slam in a large-scale environment. In *2014 IEEE International Conference on Robotics and Automation (ICRA)*, pages 1532–1539, 2014.
20. H.Strasdat, J.Montiel, and A.Davison. Scale drift-aware large scale monocular slam. volume 2, page 7, 06 2010.
21. J.Gross and T.Tucker. *Topological graph theory*. Courier Corporation, 2001.
22. J.Lee. *Smooth manifolds*. Springer, 2013.
23. J.Lim, J.Frahm, and M.Pollefeys. Online environment mapping. In *CVPR 2011*, pages 3489–3496, Colorado Springs, CO, USA, June 2011. IEEE.

24. J.Schönberger and J.Frahm. Structure-from-motion revisited. In *2016 IEEE Conference on Computer Vision and Pattern Recognition (CVPR)*, pages 4104–4113, 2016.
25. J.Shotton, B.Glocker, C.Zach, S.Izadi, A.Criminisi, and A.Fitzgibbon. Scene coordinate regression forests for camera relocalization in rgb-d images. In *2013 IEEE Conference on Computer Vision and Pattern Recognition*, pages 2930–2937, 2013.
26. J.Sprickerhof, A.Nüchter, K.Lingemann, and J.Hertzberg. An explicit loop closing technique for 6d slam. pages 229–234, 2009.
27. L.Lui, W.Zeng, ST.Yau, and X.Gu. Shape analysis of planar multiply-connected objects using conformal welding. *IEEE transactions on pattern analysis and machine intelligence*, 36(7):1384–1401, 2014.
28. M.Arie-Nachimson, S.Kovalsky, I.Kemelmacher-Shlizerman, A.Singer, and R.Basri. Global motion estimation from point matches. In *2012 Second International Conference on 3D Imaging, Modeling, Processing, Visualization Transmission*, pages 81–88, 2012.
29. M.Desbrun, E.Kanso, and Y.Tong. Discrete differential forms for computational modeling. In *Discrete differential geometry*, pages 287–324. Springer, 2008.
30. M.Desbrun, M.Meyer, and P.Alliez. Intrinsic parameterizations of surface meshes. In *Computer graphics forum*, volume 21, pages 209–218. Wiley Online Library, 2002.
31. N.Snaveley, S.Seitz, and R.Szeliski. Skeletal graphs for efficient structure from motion. In *2008 IEEE Conference on Computer Vision and Pattern Recognition*, pages 1–8, 2008.
32. O.Onur, V.Vladislav, B.Ronen, and S.Amit. A survey of structure from motion, 2017.
33. P.Purkait, T.Chin, and I.Reid. NeuRoRA: Neural Robust Rotation Averaging. In A. Vedaldi, H. Bischof, T. Brox, and J.-M. Frahm, editors, *Computer Vision – ECCV 2020*, pages 137–154, Cham, 2020. Springer International Publishing.
34. Q.Zhou and V.Koltun. Dense scene reconstruction with points of interest. *ACM Transactions on Graphics*, 32:1–8, 07 2013.
35. R.Bott and L.Tu. *Differential Forms in Algebraic Topology*, volume 82. Springer, 1982.
36. R.Hartley, J.Trumpf, Y.Dai, and H.Li. Rotation averaging. *International Journal of Computer Vision*, 103:267–305, 2012.
37. R.Hartley, K.Aftab, and J.Trumpf. L1 rotation averaging using the weiszfeld algorithm. In *CVPR 2011*, pages 3041–3048, 2011.
38. R.Mur-Artal and J.Tardós. Fast relocalisation and loop closing in keyframe-based slam. In *2014 IEEE International Conference on Robotics and Automation (ICRA)*, pages 846–853, 2014.
39. R.Newcombe, S.Izadi, O.Hilliges, D.Molyneaux, D.Kim, A.Davison, P.Kohi, J.Shotton, S.Hodges, and A.Fitzgibbon. Kinectfusion: Real-time dense surface mapping and tracking. In *2011 10th IEEE International Symposium on Mixed and Augmented Reality*, pages 127–136, 2011.
40. S.Krishnan, P.Lee, J.Moore, and S.Venkatasubramanian. Global registration of multiple 3d point sets via optimization-on-a-manifold. pages 187–196, 01 2005.
41. S.Lando, A.Zvonkin, and D.Zagier. *Graphs on surfaces and their applications*, volume 75. Springer, 2004.

42. T.Duchamp, A.Certain, A.DeRose, and W.Stuetzle. Hierarchical computation of pl harmonic embeddings. *preprint*, 1997.
43. T.Whelan, H.Johannsson, M.Kaess, J.Leonard, and J.McDonald. Robust real-time visual odometry for dense rgb-d mapping. In *2013 IEEE International Conference on Robotics and Automation*, pages 5724–5731, 2013.
44. V.Govindu. Lie-algebraic averaging for globally consistent motion estimation. In *Proceedings of the 2004 IEEE Computer Society Conference on Computer Vision and Pattern Recognition, 2004. CVPR 2004.*, volume 1, pages 1–8, 2004.
45. V.Govindu. Robustness in motion averaging. In *Asian Conference on Computer Vision*, pages 457–466. Springer, 2006.
46. V.Govindu and A.Pooja. On averaging multiview relations for 3d scan registration. *IEEE Transactions on Image Processing*, 23(3):1289–1302, 2013.
47. X.Gu and ST.Yau. Global conformal surface parameterization. In *Proceedings of the 2003 Eurographics/ACM SIGGRAPH symposium on Geometry processing*, pages 127–137, 2003.